The background image shows a rugged, mountainous landscape. In the foreground, there is a rocky, gravelly path or road. The middle ground features a valley with some sparse vegetation and a small structure. The background consists of large, steep mountains under a blue sky with light clouds.

EGU2020-5939

**Synthetic aperture radar
coherence as a proxy for
geomorphic activity**

**Stephanie Olen
Bodo Bookhagen**

EGU General Assembly 2020
Sharing Geoscience Online

Hillslope Processes

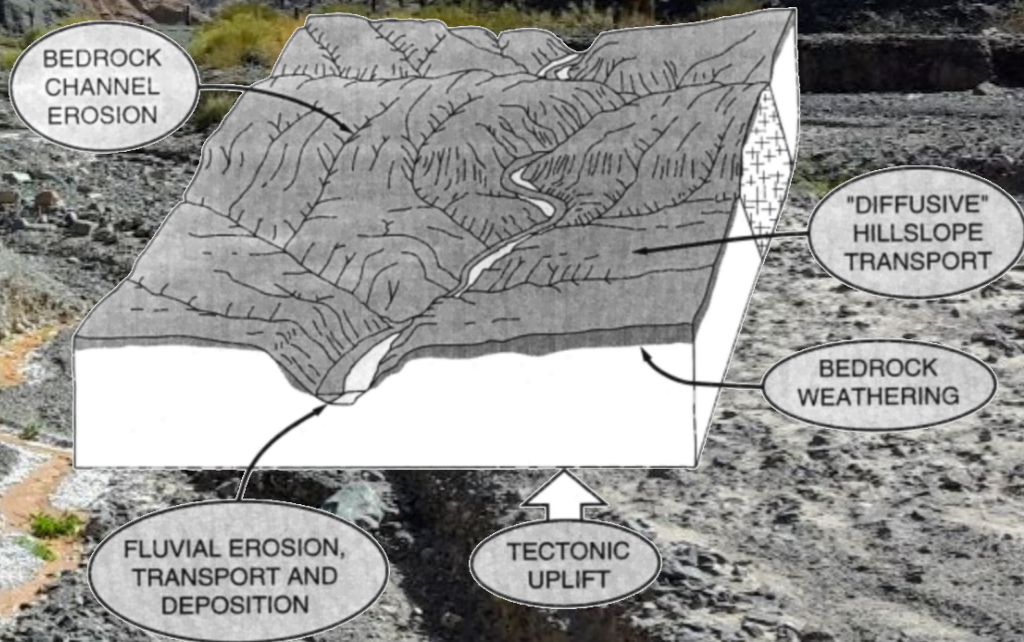
Regional Climate

Fluvial Incision

Tectonics

Biota

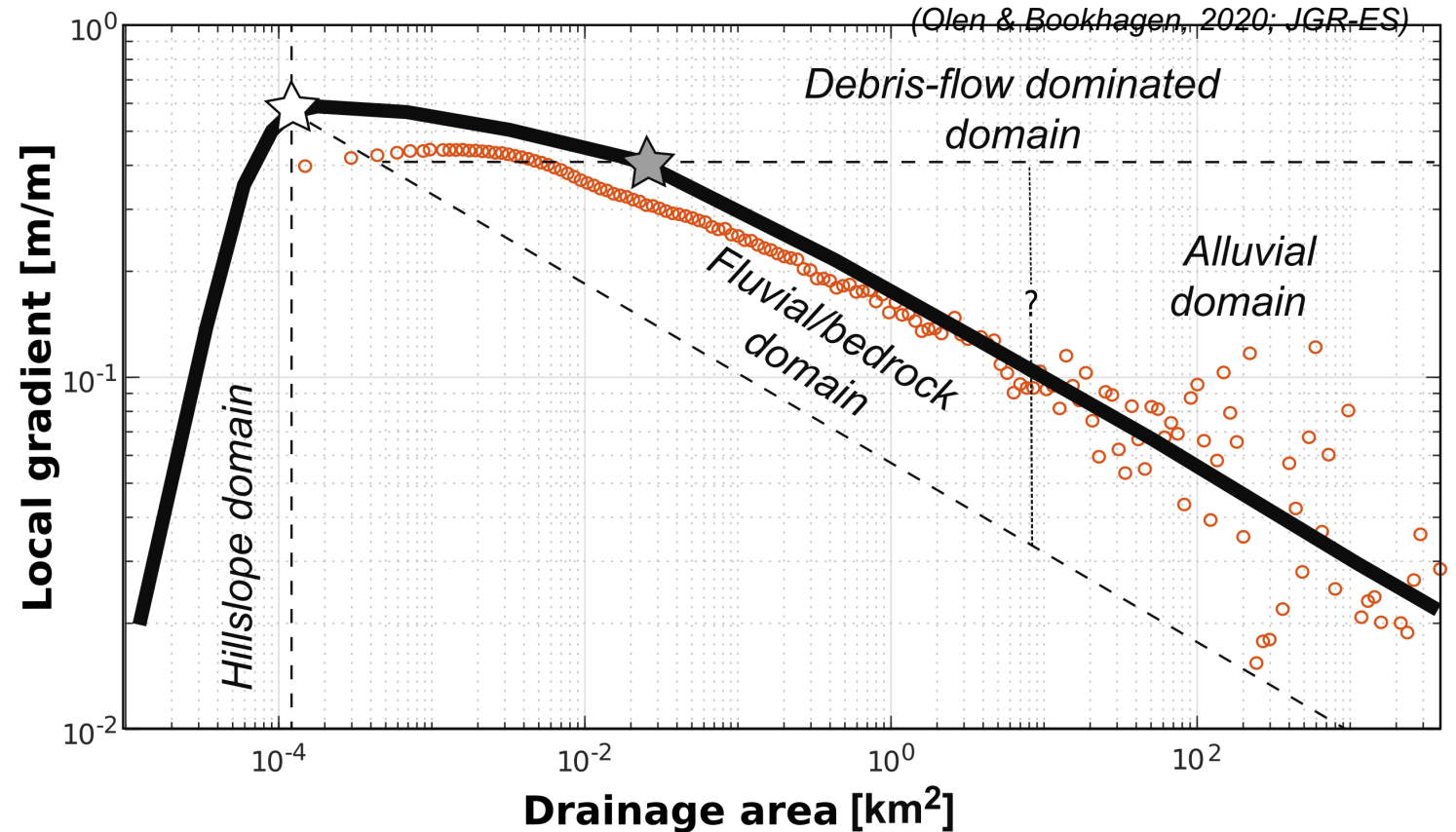
Alluvial Transport



Transitions in sediment transport domains

Transition between transport domains has traditionally been determined from high-resolution topography (e.g., from lidar surveys), based on inflections in the relationship between increasing **drainage area [km²]** and local **topographic gradient [m/m]**.

However, this analysis is highly resolution-dependent and sufficiently high-resolution digital elevation models are not widely available.

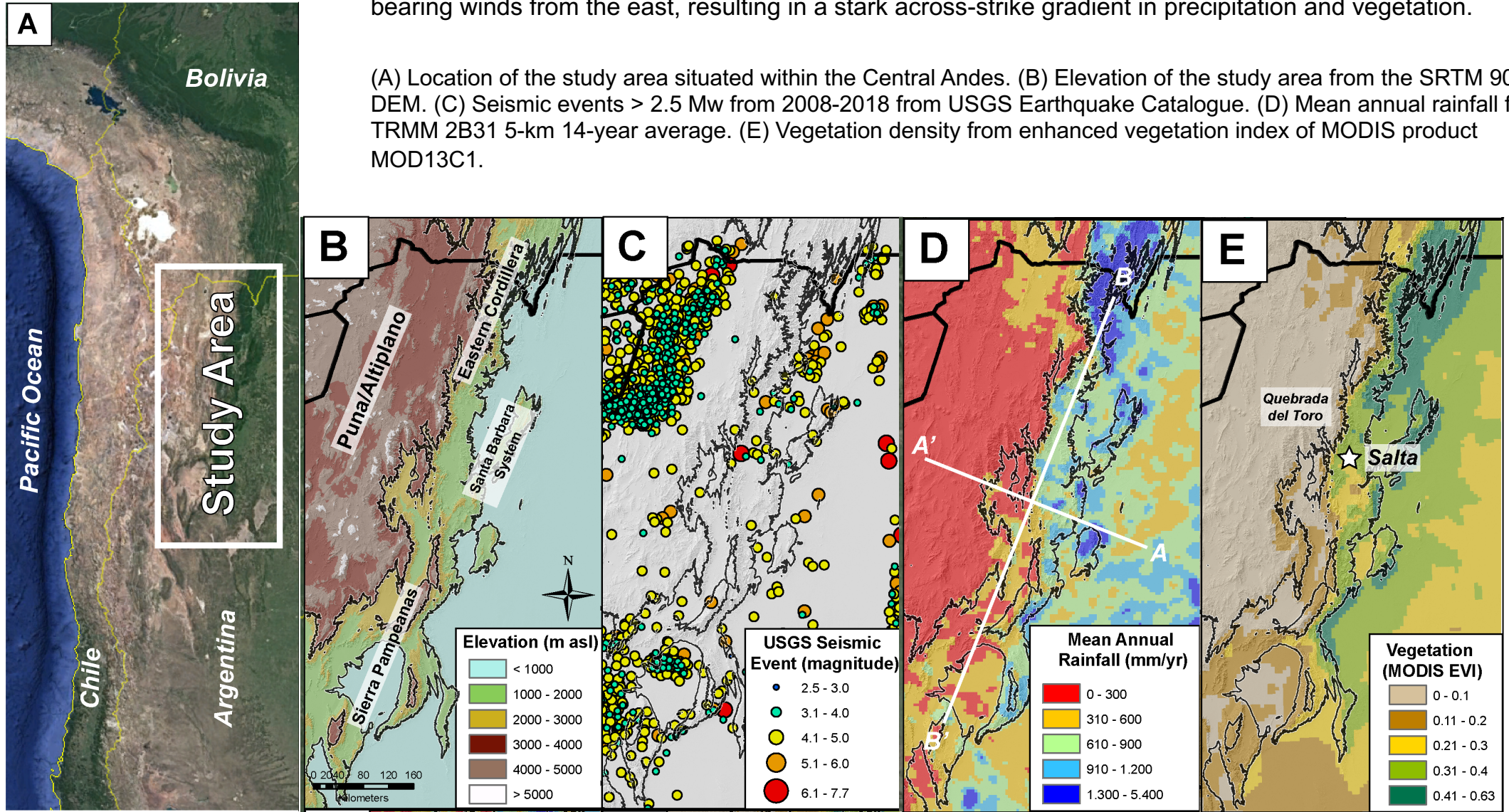


Theoretical relationship (thick black line) between increasing drainage area and local river channel gradient, delineating the boundaries between transport domains, after Tarolli and Fontana (2009) and Montgomery and Foufoula-Georgiou (1993). Binned median channel gradient and drainage area from the Quebrada del Toro shown in orange.

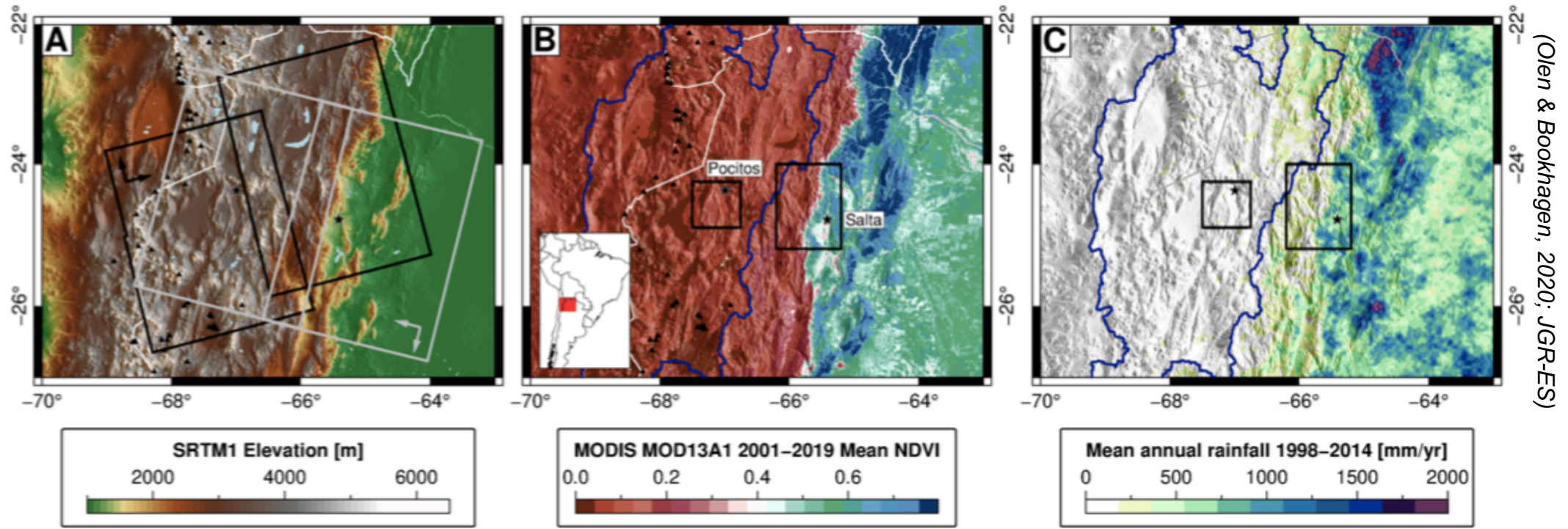
Regional Setting: South-central Andes

The south-central Andes are a tectonically active, subduction-driven mountain range. The eastern flanks of the orogen are seismically active and characterized by reactivated normal faults in a broken foreland system. The north-south strike of the south-central ranges are perpendicular to the predominant moisture-bearing winds from the east, resulting in a stark across-strike gradient in precipitation and vegetation.

(A) Location of the study area situated within the Central Andes. (B) Elevation of the study area from the SRTM 90-m DEM. (C) Seismic events > 2.5 Mw from 2008-2018 from USGS Earthquake Catalogue. (D) Mean annual rainfall from TRMM 2B31 5-km 14-year average. (E) Vegetation density from enhanced vegetation index of MODIS product MOD13C1.



Study area: South-central Andes in NW Argentina

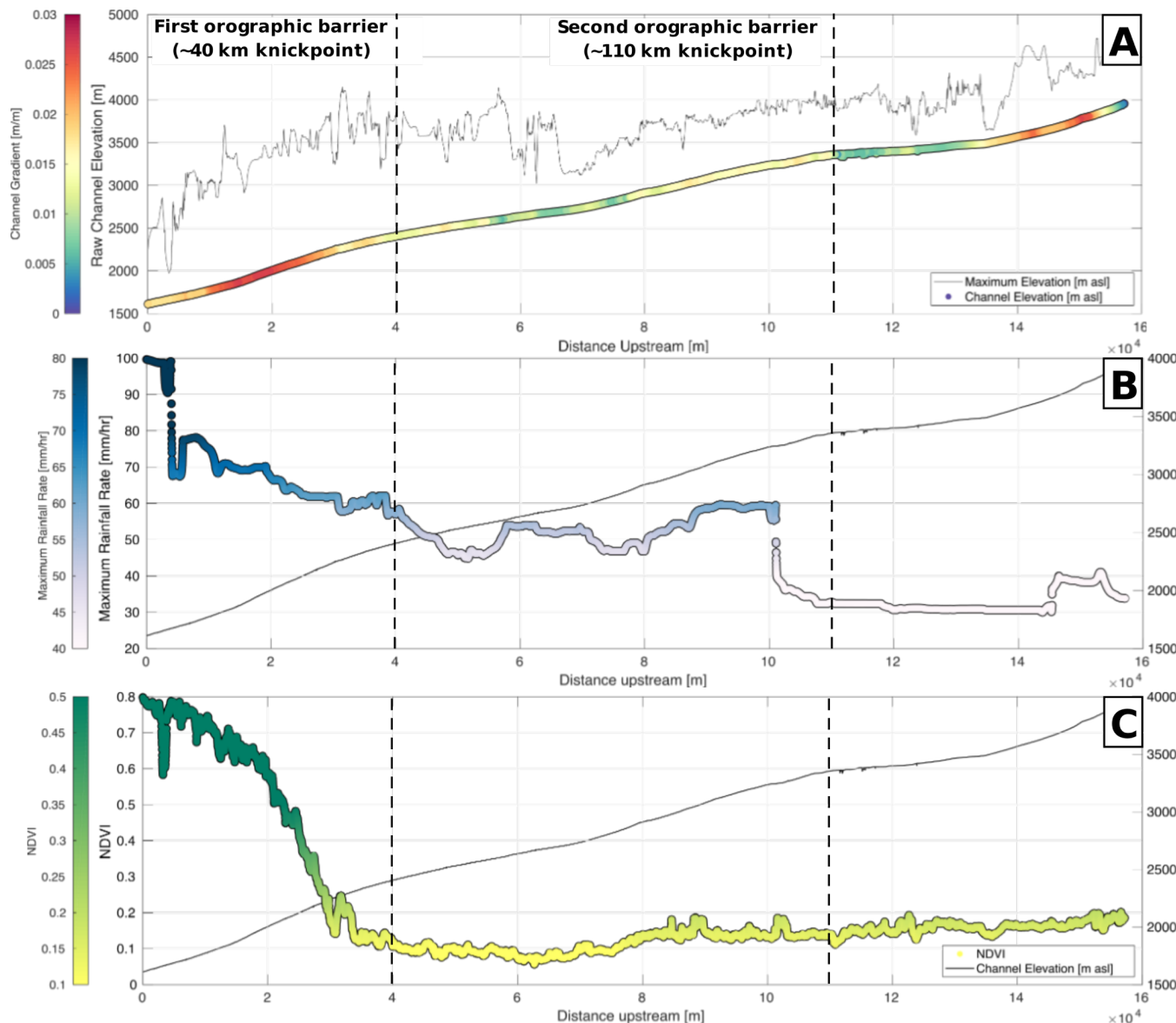


(A) **Elevation** of the region of interest. Footprints of the Sentinel-1 IW SLC images used are shown in grey for the descending tracks (10, 83) and black for the ascending tracks (76, 149), with arrows for corresponding flight and look directions.

(B) **Vegetation density** from the **MOD13Q1** 250-m normalized difference vegetation index (NDVI), demonstrating the stark gradient of vegetation and precipitation, which are positively correlated, within our study area. Location of specific regions of interest are shown in black boxes: the Pocitos region in the orogenic interior (Puna Plateau) and the Quebrada del Toro in the intermontane basins.

(C) **Rainfall** in the region follows a similar pattern (Bookhagen & Strecker, 2008, 2012), with precipitation focused in the eastern foreland with occasional penetration into the intermontane basins, and rare rainfall events on the Puna Plateau. The regions where analyses are carried out are outlined in polygons (b, c) with an eastern box centered on the intermontane basins (Quebrada del Toro region, near the city of Salta) and a western box in the central Puna Plateau (Pocitos region).

Transport characteristics across regional gradients



The Quebrada del Toro typifies the gradients found within the south-central Andes. Along the course of the Quebrada del Toro, swath profiles show these gradients:

(A) **Raw channel elevation** colored by **channel gradient [m/m]** and maximum elevation along the river channel. Two prominent knickpoints in the channel, at ~40 km and ~110 km upstream of the outlet that correspond to the first and second orographic barriers within the Quebrada del Toro basin.

(B) **Maximum monthly precipitation rate [mm/hr]** derived from the Global Precipitation Measurement Mission (Hou et al., 2014; Smith et al., 2007).

(C) **Vegetation density** from the normalized difference vegetation index (**NDVI**) calculated from Landsat-8 multispectral imagery.

Maximum elevation, GPM precipitation, NDVI, and coherence were calculated from a 500-m swath along the course of the river.

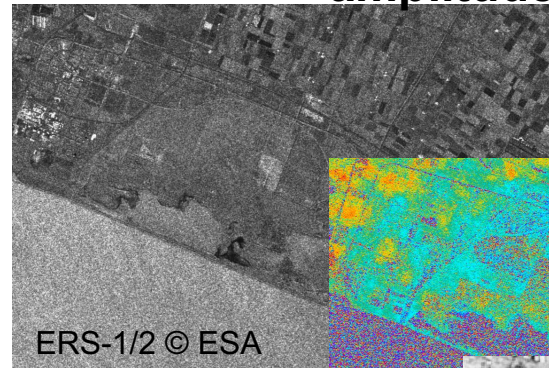
(Olen & Bookhagen, 2020; JGR-ES)

Synthetic Aperture Radar (SAR) Coherence

SAR images are composed of a **phase** and **amplitude** signal, which give information about the distance and intensity of the received radar wave, respectively.

Coherence measures the **correlation** between two SAR images (phase and amplitude/intensity) from one location imaged at two (or more) different times.

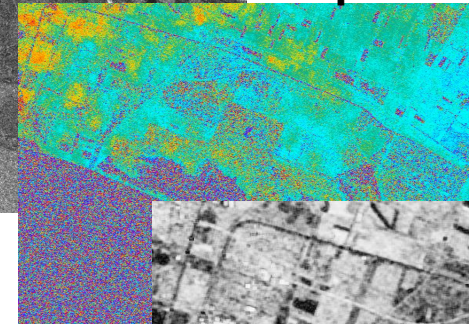
Time 1



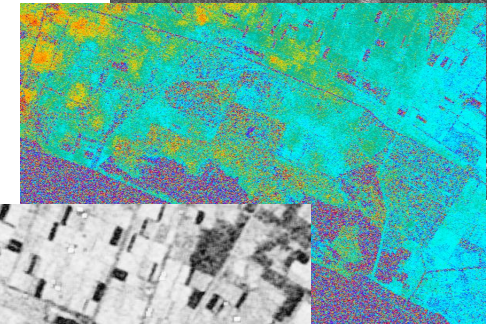
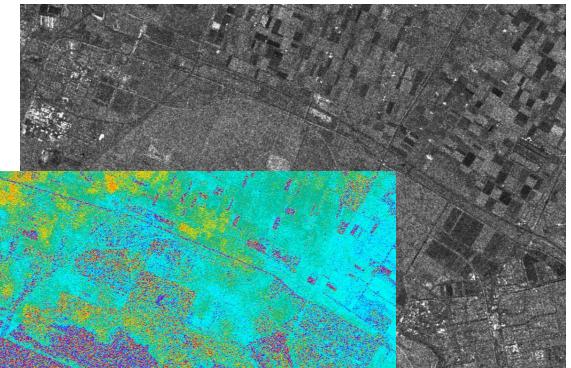
Flevoland, NL

amplitude

phase



Time 2



coherence

Coherence = 1 →

No surface change or signal degradation

Coherence < 1 → Change in phase or amplitude of radar signal

SAR data acquisition and processing

Sentinel-1 SAR Single Look Complex (SLC) Interferometric Wide (IW) images used:

Region ^a	Track ^b	Orbit ^c	Start date ^d	End Date ^e	Number of SAR images ^f
Quebrada del Toro	Track 76	Ascending	27 November 2014	28 February 2019	70
	Track 10	Descending	11 November 2014	8 March 2019	80
Pocitos	Track 149	Ascending	27 October 2014	15 February 2019	119
	Track 83	Descending	23 October 2014	25 March 2019	79

Note. Detailed list of all SAR data used is given in Table S1.
^aStudy area region as outlined in Figure 3. ^bAcquisition track number. ^cSatellite direction. ^dDate of the first SAR image of the track time series. ^eDate of the last SAR image of the track time series. ^fTotal number of images for a given track in the time series.

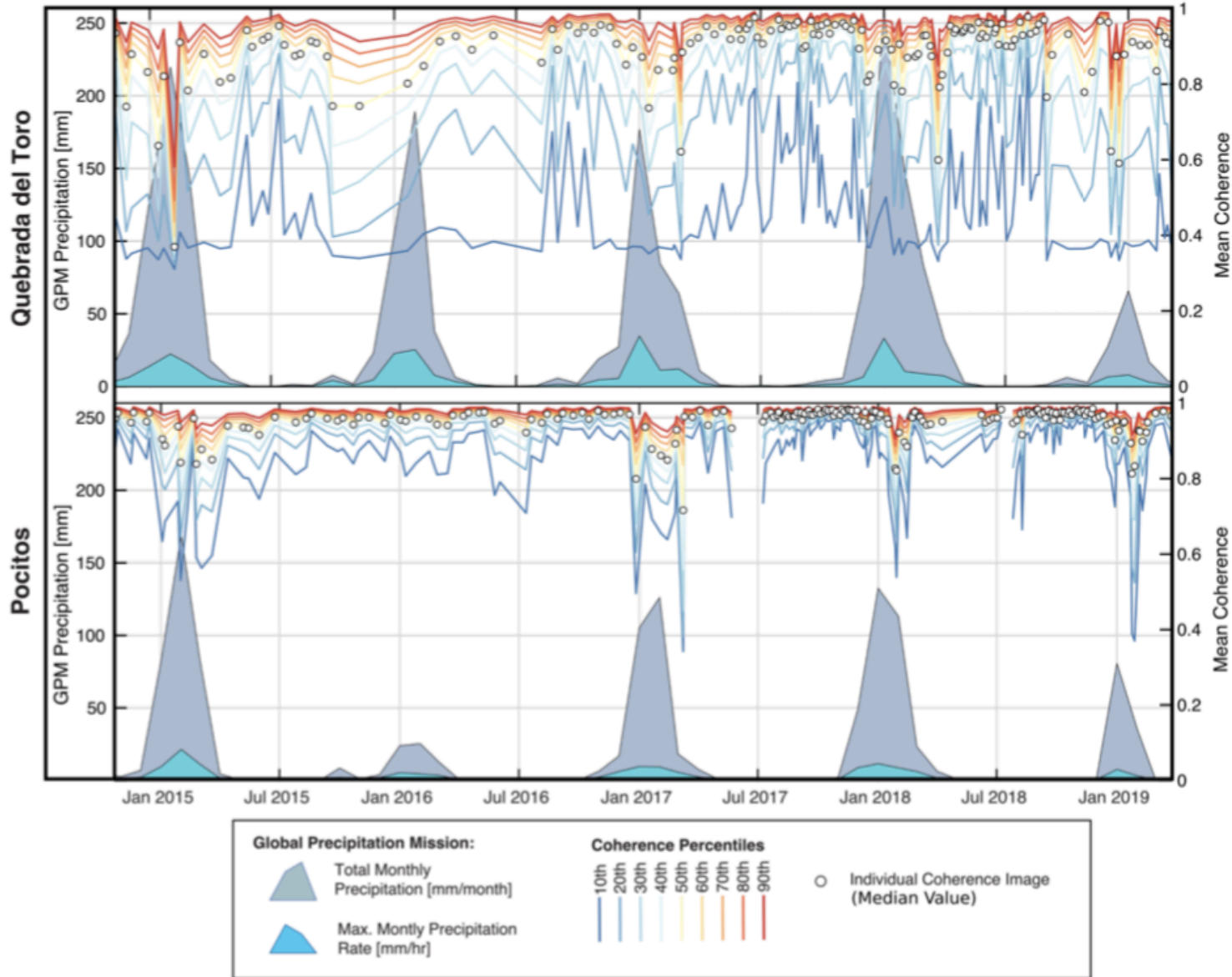
Sentinel-1 images were acquired through ESA's Copernicus Open Access Science Hub. Coherence images were coregistered and calculated pairwise between SAR images using the InSAR Scientific computing Environment (ISCE; Rosen et al., 2011).

Regions masked out:

- *Surface incidence angle < 60 degrees (topographic shadowing).*
- *NDVI (Normalised Difference Vegetation Index) greater than 0.3 (LANDSAT-8 30-m NDVI using three year greenest pixel average).*
- *Regions with high ∂ Amplitude $>2\sigma$ to serve as a soil moisture proxy*

Ascending and descending images are amalgamated into a single stack and seasonal (NDJFMA) and annual averages are calculated.

Coherence time series and seasonality



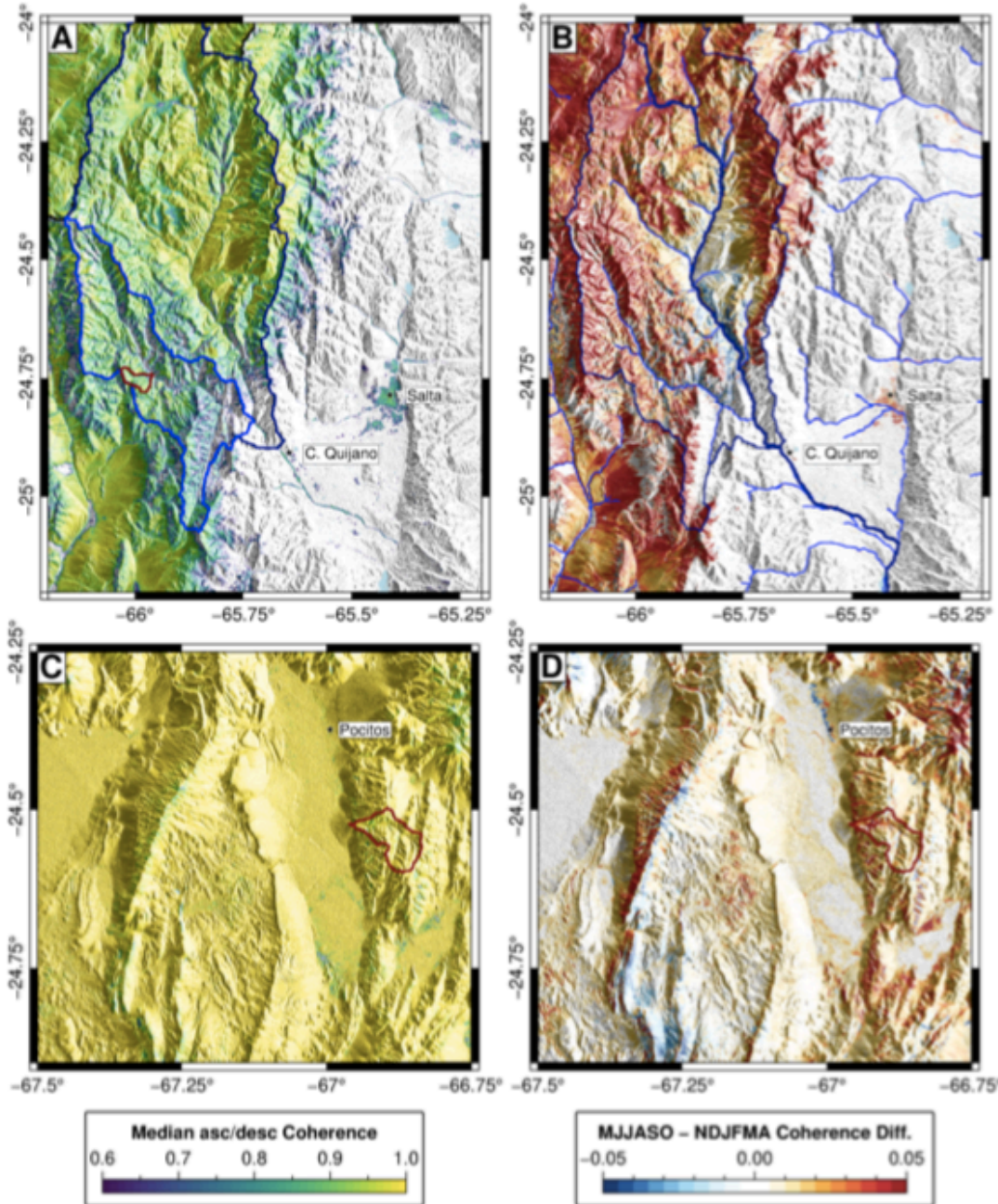
Coherence and **precipitation** vary seasonally in the Quebrada del Toro and the Pocitos region.

We observe a **negative correlation between precipitation and coherence**, with lowest coherence during the austral summer (NDJFMA) when the majority of rainfall occurs. This suggests that **the majority of sediment transportation takes place during the regional wet-season.**

Monthly total precipitation [mm/month] and **maximum precipitation rate [mm/hr]** are taken from the Global Precipitation Measurement (GPM) Mission.

Coherence and precipitation are averaged over the entire Quebrada del Toro and Pocitos regions for each date.

Coherence spatial patterns



(Olen & Bookhagen, 2020; JGR-ES)

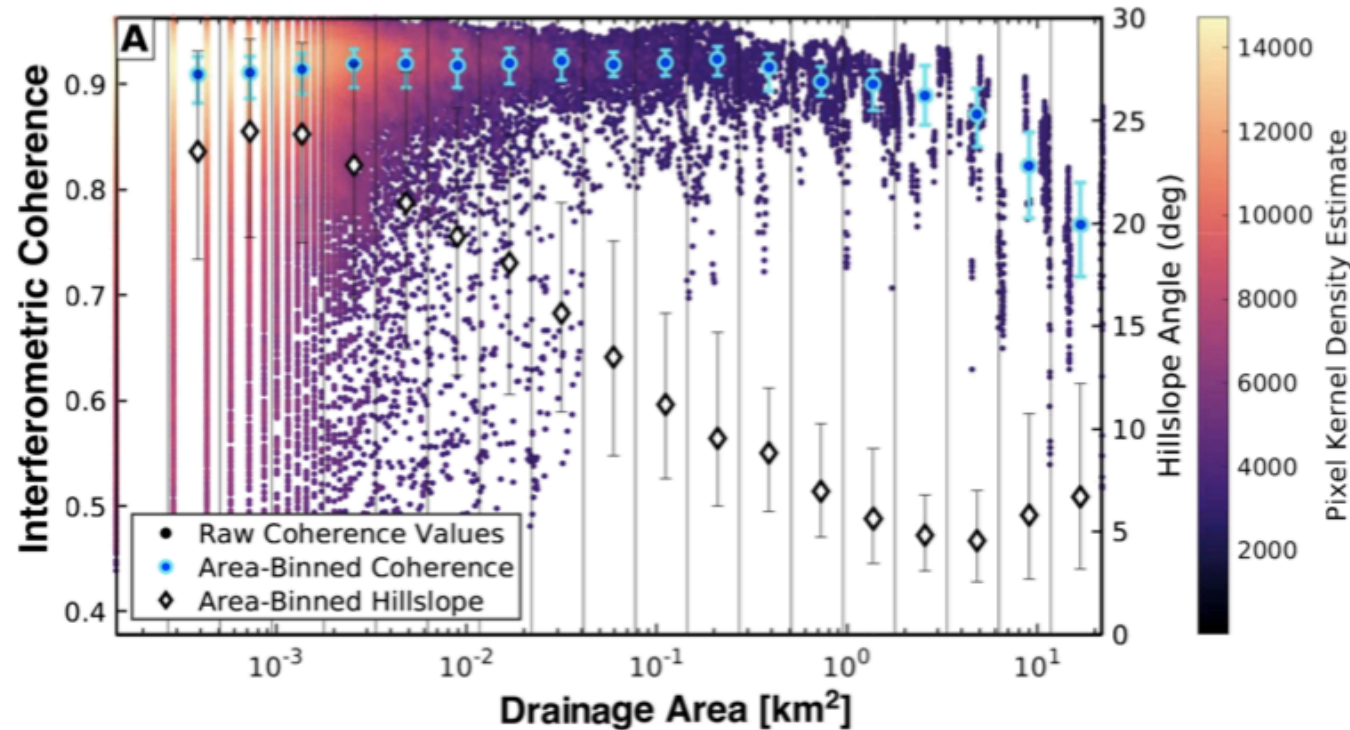
- Coherence is generally high across arid and semiarid landscapes.
- Discrete areas of low coherence on high elevation peaks (potential snowfall),
- Concentrated low coherence in the Rio Capilla (southern tributary to the Quebrada del Toro).
- MJJASO/NDJFMA ratio highest on steep mountain slopes, suggesting that debris flows and other hillslope sediment transport are primarily occurring during the wet season.

Interferometric coherence of the two study areas from the combined ascending and descending tracks. Areas with significant vegetation cover ($NDVI > 0.3$) have been masked out.

A and C show the **median coherence** for each region over the observation period from October 2014 – February 2018 ($n=97$ pairs for the Quebrada del Toro; $n = 135$ pairs for the Pocitos basin). **B and D** show the ratio of the dry-season austral winter (MJJASO) to the wet-season austral summer (NDJFMA) coherence (MJJASO/NDJFMA), with **ratios greater than 1 representing higher coherences during the dry season**. This occurs because the landscape has a greater degree of geomorphic activity during the wet season.

Sediment transport domains: transition detection

(Olen & Bookhagen, 2020; JGR-ES)



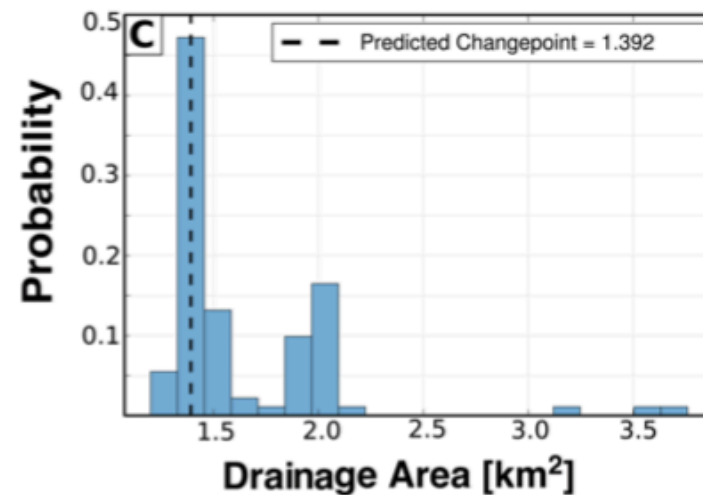
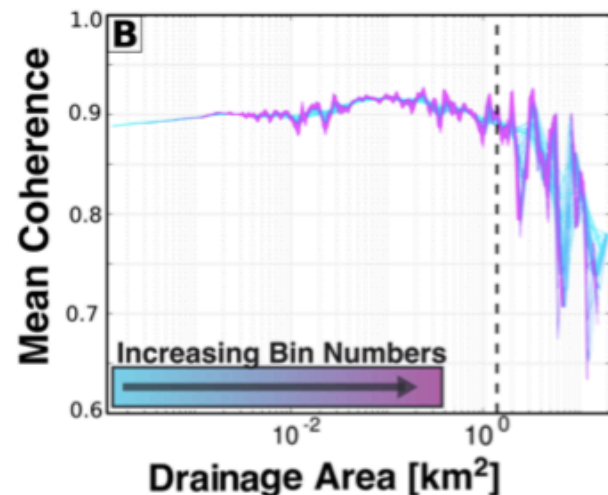
Change point detection in area-coherence relationship:

- 1) Bin coherence values by drainage area in log-spaced bins (A).
- 2) Calculate relevant statistics of each bin (percentile range [95th – 5th], skewness, standard deviation, median, mean) (A).
- 3) Perform change point analysis based on cumulative sums (Taylor, 2000).

a) Repeat with multiple bin numbers (20-200 bins), including all samples in each bin (B).

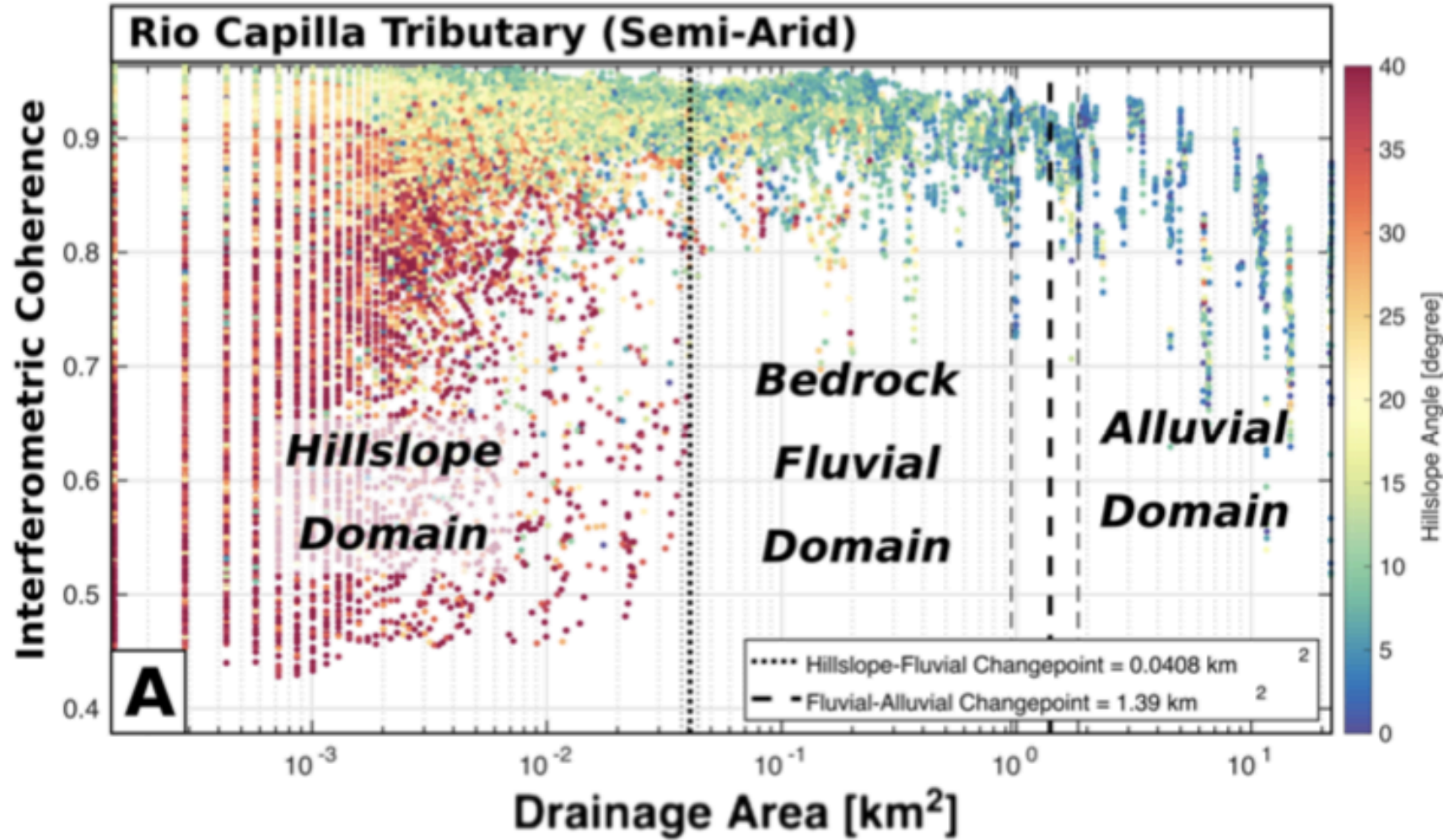
b) Set single bin number (e.g., 100) and use bootstrapping to subsample the dataset.

c) Calculate most probable change point from ensemble of predicted change point locations (C).



Sediment transport domains change points

(Olen & Bookhagen, 2020; JGR-ES)



First change point:

Small drainage areas with low coherence values and high hillslopes (above critical hillslope angle of ~30 deg).

→ Transition from hillslope transport processes to fluvial transport processes

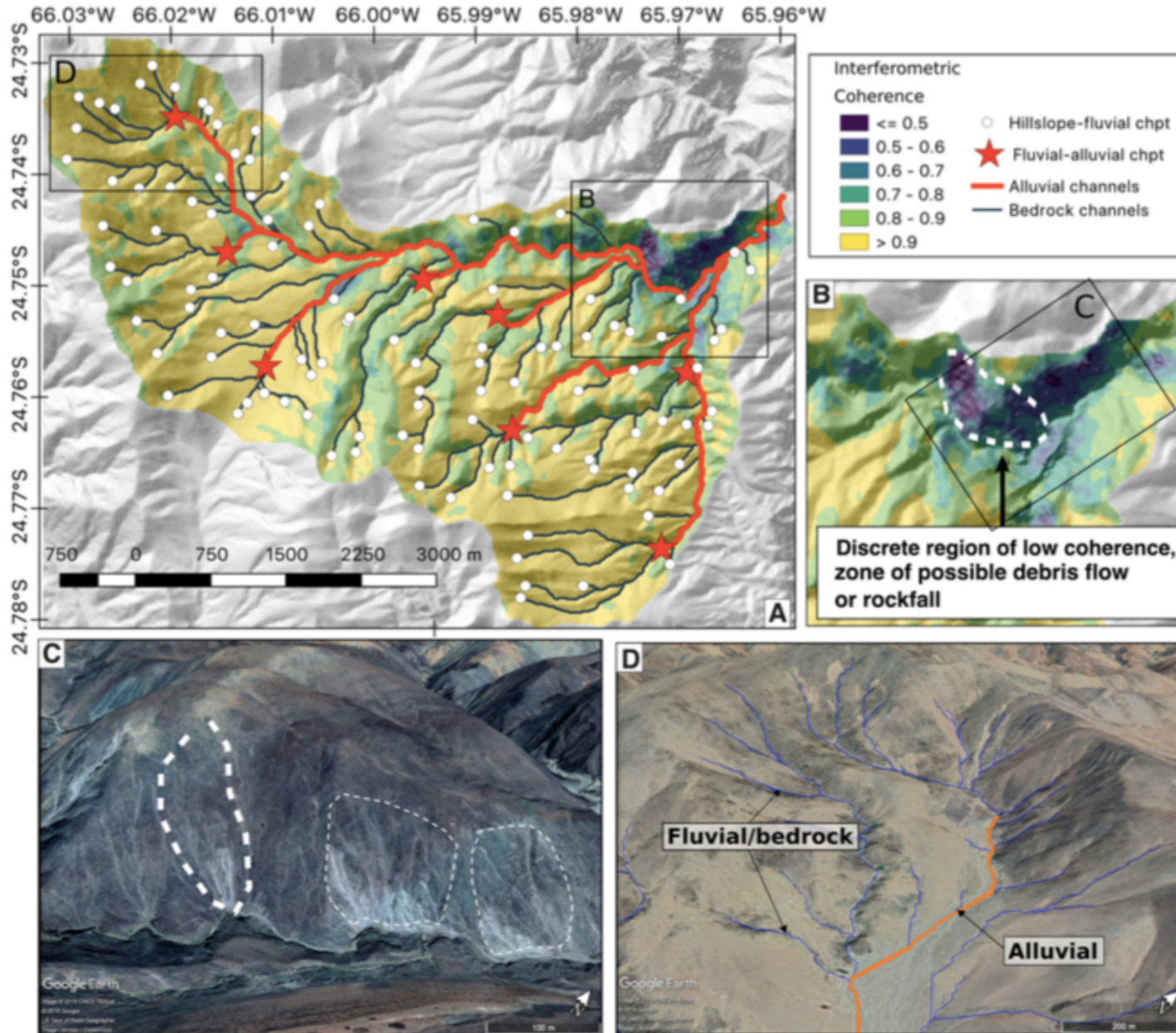
Second change point:

Decrease in mean coherence as drainage area increases and hillslope angles decrease.

→ Transition between fluvial channels and sediment-filled alluvial channels

Mapping transport domain change points

Interpretation

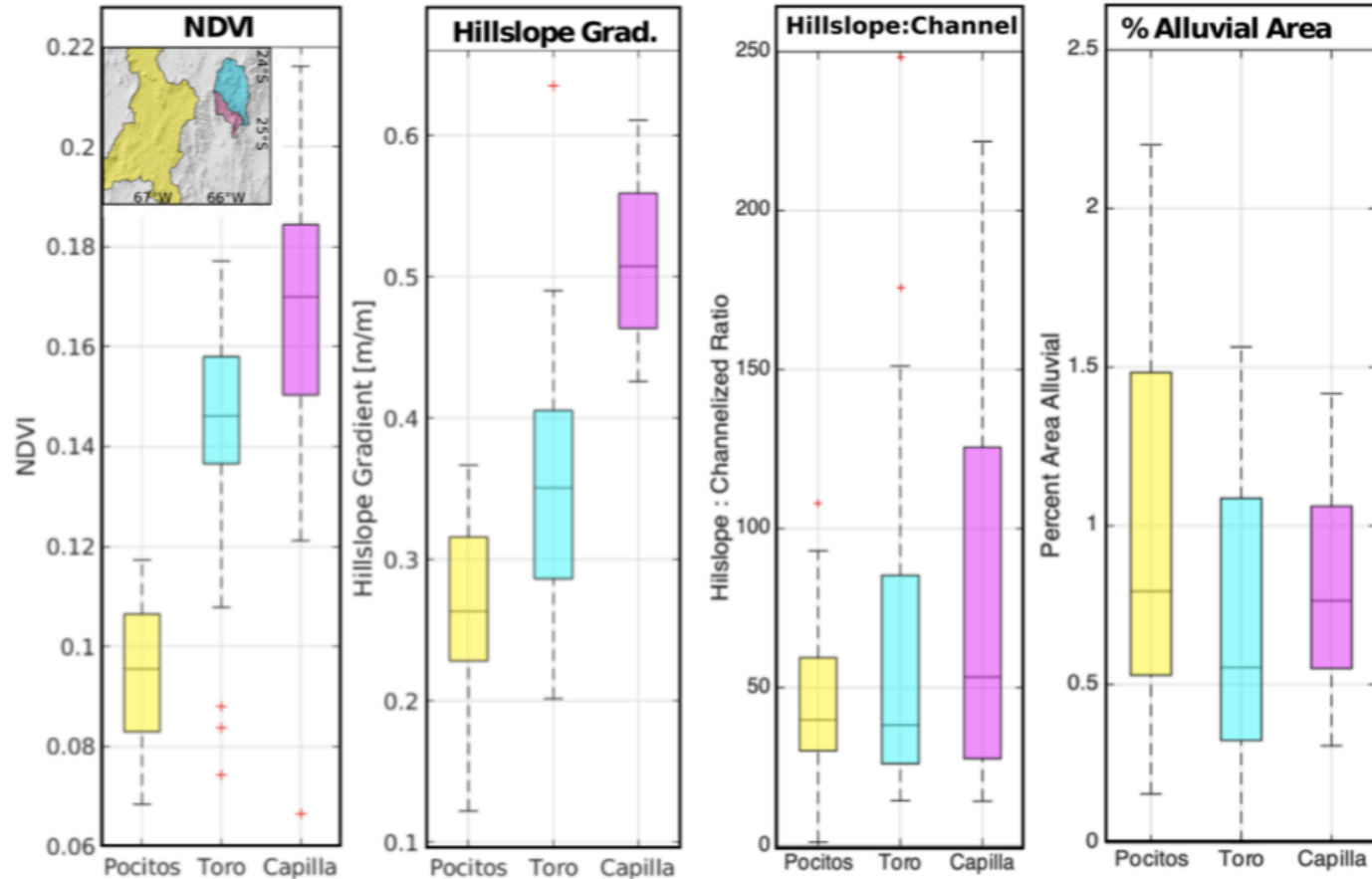


Example of coherence and **change point detection** on a tributary to the Rio Capilla. (A) Average coherence for a tributary to the Rio Capilla. The detected change points are mapped onto the basin (**hillslope-fluvial**, white circles; **fluvial-alluvial**, red stars) along with the corresponding fluvial/bedrock and alluvial/sediment-laden portions of the river network (blue and orange, respectively).

(B) Detail of the coherence from a high-relief zone within the basin **prone to debris flow** and rockfall, where discrete patches of low coherence likely represent sediment movement on **landslide scarps** (C). (D) Example of the **fluvial and alluvial transport domains** as extracted from the change point analysis super imposed on Google Earth imagery.

Transport characteristics across regional gradients

Interpretation



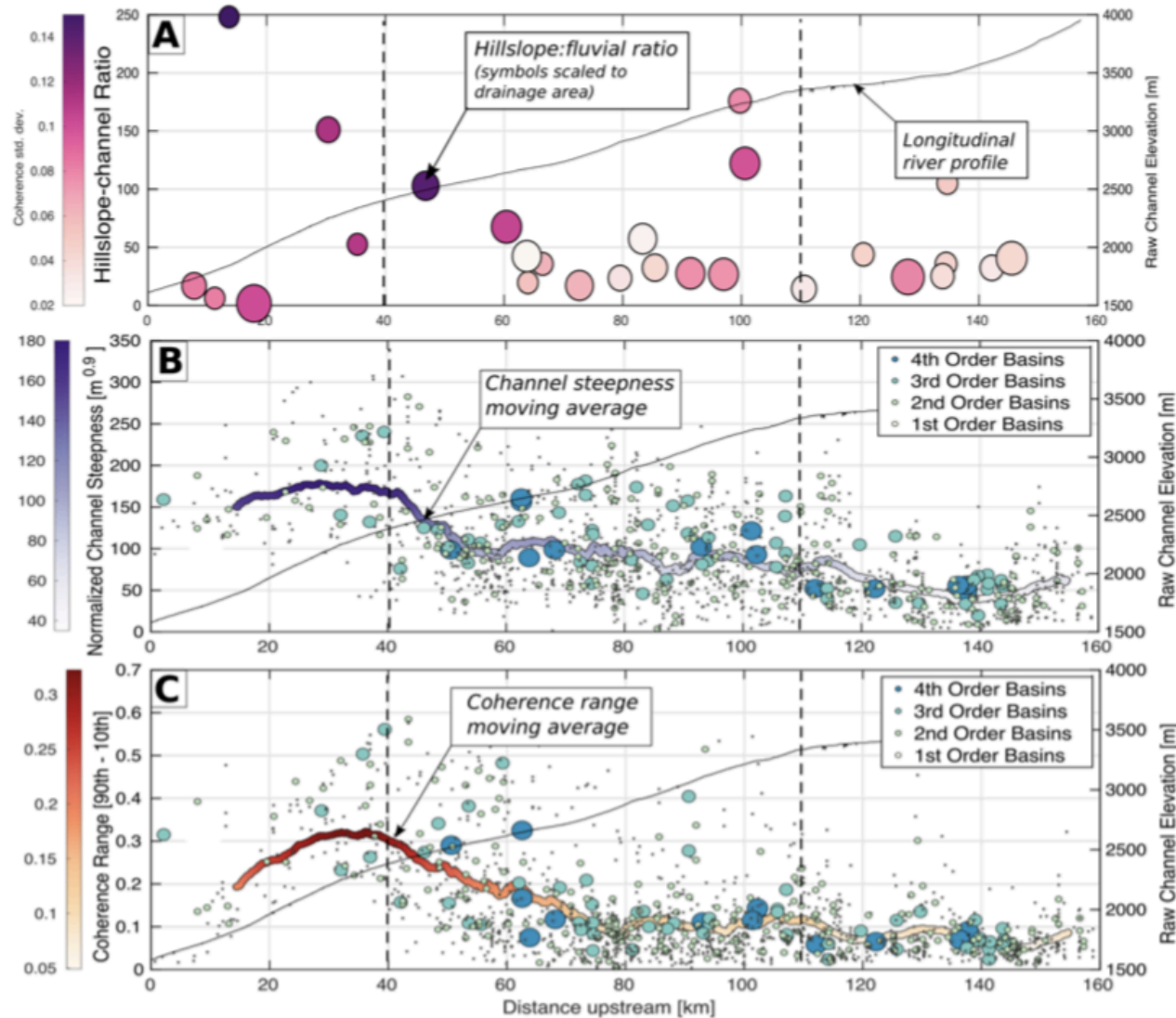
(Olen & Bookhagen, 2020; JGR-ES)

Characteristic results of each region: **Pocitos** (yellow, N = 58), **Quebrada del Toro** (blue, N = 35), and **Rio Capilla** (pink; subdivided large tributary to Quebrada del Toro, N = 18) basins. Boxplots show median, interquartile range (25th and 75th percentiles), and outliers (10th and 90th percentiles). **NDVI from a 4-year greenest pixel average** of Landsat-8 images from the observation period (2015–2019). **Hillslope gradient** calculated from Tandem-X 12- m research DEM. The **ratio of hillslope-to-fluvial domain** (equation below) shows a clear increase from the more arid, gentler Pocitos region toward the steeper, wetter, and more vegetated Rio Capilla. This is reflected in the percent decrease of each basin in the fluvial and **alluvial transport domain**, which are highest in the Pocitos region where channels more rapidly transition into sediment-filled alluvial channels.

$$\text{Hillslope:Fluvial Ratio } (R_{HF}) = \frac{\text{Area above HF change point}}{\text{Area between HF and FA change points}}$$

Transport characteristics across regional gradients

Interpretation



River long profile of the Quebrada del Toro, showing

(A) **Ratio of hillslope-fluvial domain (R_{HF})** in every tributary larger than 10 km² draining into the Rio Toro, colored by the standard deviation of wet-season coherence within that basin.

(B) **Normalized channel steepness (ks_n)**. Channel steepness index (ks_n), a geomorphic metric for long-term erosion rates, is highest in the lower Quebrada del Toro, where erosion is greatest (Bookhagen & Strecker, 2012; Tofelde et al., 2018).

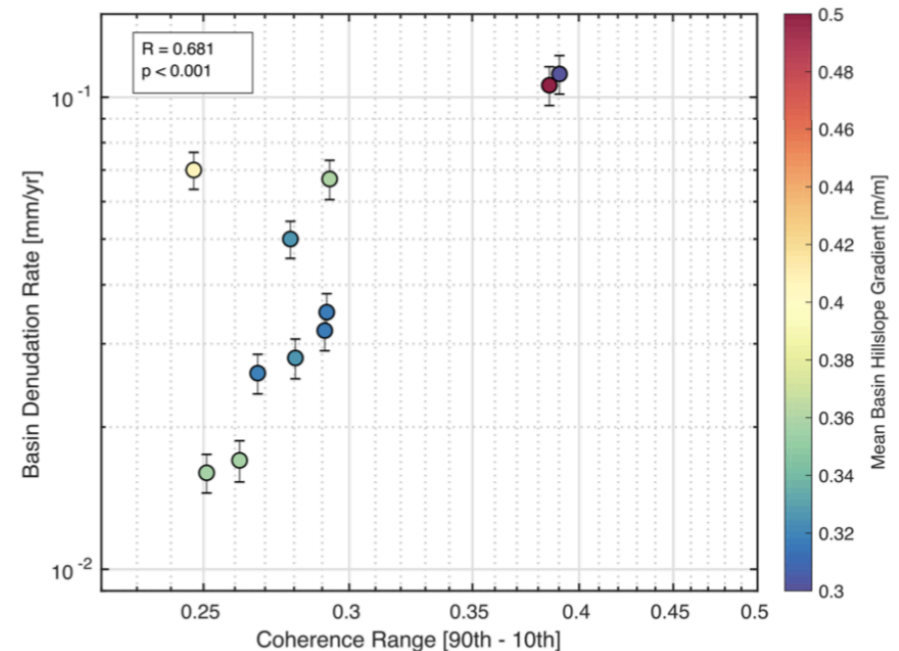
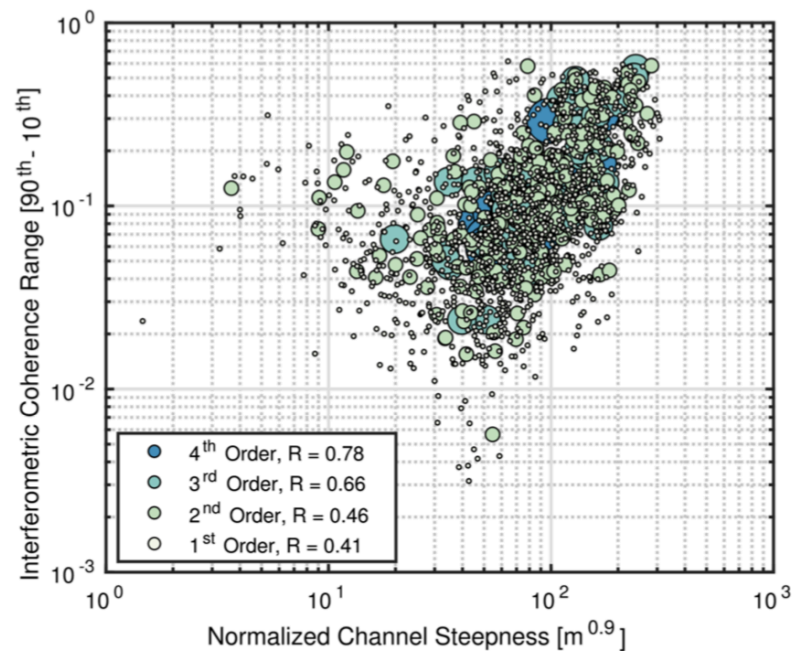
(C) **Coherence range** (90th - 10th percentile) of each basin. The range of coherence values in this region are also highest, decreasing in the more geomorphically stable upper Quebrada del Toro.

(B) and (C) are calculated for **every first, second, third, and fourth order basin** within the Quebrada del Toro with a minimum basin size of 1 km².

(Olen & Bookhagen, 2020; JGR-ES)

Coherence range and landscape stability

Relationship between **channel steepness (ks_n)** and the **coherence range (90th – 10th percentile)** in basins across the **Quebrada del Toro**. Though non-linear, the positive correlation ks_n and coherence range suggests a relationship between landscape timescale and monthly to annual (measured by coherence) geomorphic activity in the study area. Wherein a low coherence range occurs predominantly in watersheds that are stable during the observation period and show geomorphic indication of low geomorphic activity. Basins with **high coherence range represent less stable basins** with a higher degree of short-term geomorphic activity, and a corresponding higher long-term erosion rate.

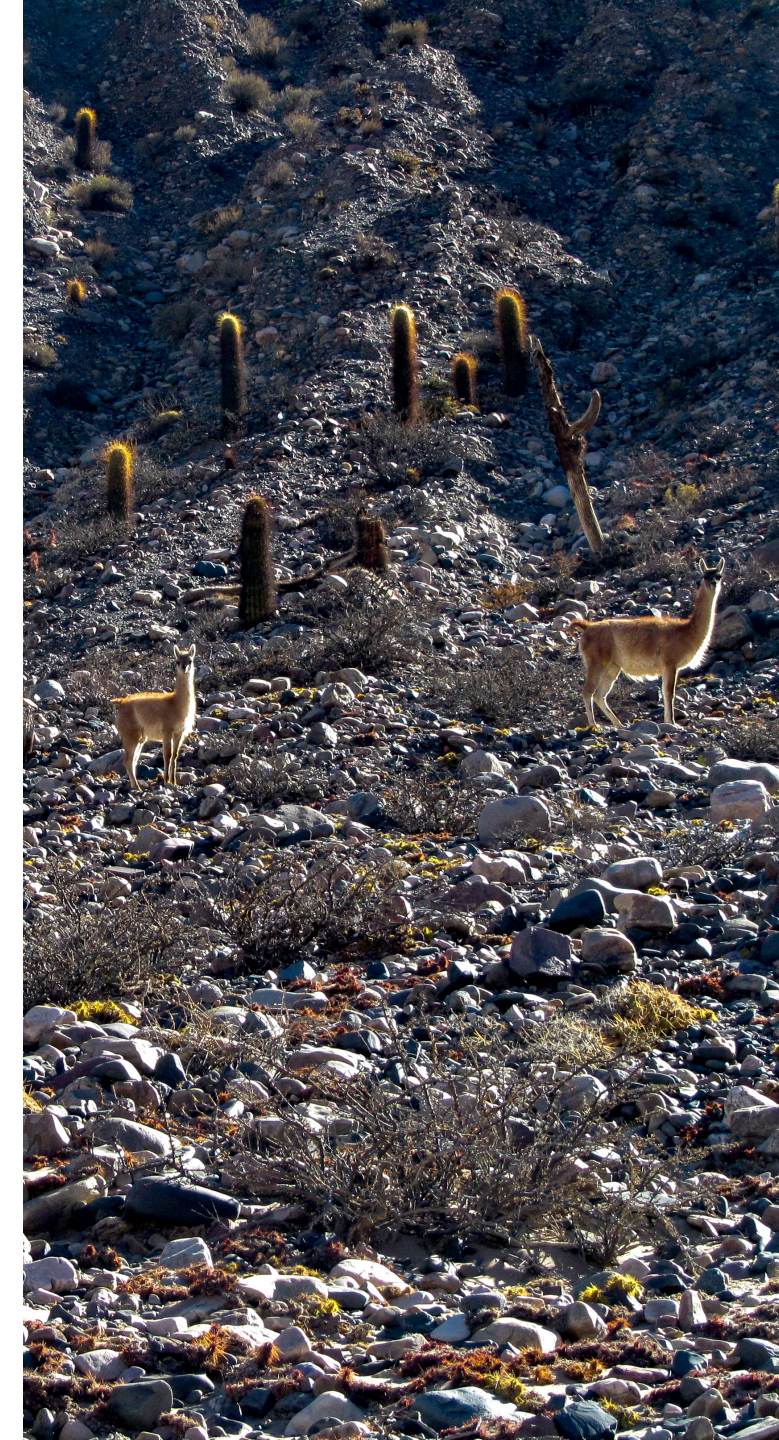


(Olen & Bookhagen, 2020; JGR-ES)

Positive relationship between **millennial denudation rates** measured from terrestrial cosmogenic 10-Beryllium (Bookhagen and Strecker, 2012; Tofelde et al., 2018) and **short-term landscape stability** measured from coherence range within each basin. Basins are colored by mean hillslope gradient within each basin [m/m], demonstrating a relationship between short-term landscape stability and long-term erosion that does not depend on basin morphology. Note that 6 basins (not shown) with high vegetation cover from these studies were removed from this analysis.

Conclusions

- 1) Interferometric SAR coherence can provide a **powerful tool for measurement sediment movement and landscape stability** across broad and inaccessible regions.
- 2) In this study, we have demonstrated that SAR coherence is sensitive to sediment movement and transport, both on hillslopes and in alluvial channels, in **arid and semi-arid environments**. This provides a new method of detecting events such as hillslope movements in arid environments, where hillslope activity may not be visible using multispectral optical images in the absence of vegetation. The coherence within a basin, because it is sensitive to different types of sediment transport throughout the basin, can be used to predict the transitions between hillslope/debris-flow dominated sediment transport and fluvial sediment transport, and from bedrock fluvial to sediment-choked alluvial domains.
- 3) In the study area in the south-central Andes, we observe a transition from hillslope-dominated to increasingly fluvially- and alluvially-dominated basin transport domains from the wetter, more vegetated to the arid, abiotic basins of the orogen interior.
- 4) The **range of coherence** within a basin can be used a proxy for **short-timescale geomorphic activity** scales to long-timescale geomorphic activity from both topographic analysis (ksn) and from millennial erosion rates derived from ^{10}Be TCN. We suggest that the range of SAR coherence can serve as an additional and independent tool to compare geomorphic activity at various timescales, particularly in regions where direct ground or field measurements are lacking.
- 5) As an increasing amount of SAR data becomes available in the future, at improved spatial resolutions and expanded radar wavelengths, SAR coherence will provide valuable and widely applicable insight into the dynamics of Earth's surface.

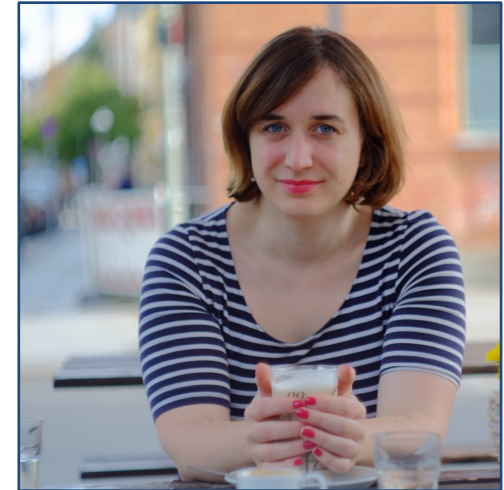


Reference & Contact

- Bookhagen, B., & Strecker, M. R. (2008). Orographic barriers, high-resolution TRMM rainfall, and relief variations along the eastern Andes. *Geophysical Research Letters*, 35(6).
- Hain, M. P., Strecker, M. R., Bookhagen, B., Alonso, R. N., Pingel, H., & Schmitt, A. K. (2011). Neogene to Quaternary broken foreland formation and sedimentation dynamics in the Andes of NW Argentina (25°S). *Tectonics*, 30, TC2006. <https://doi.org/10.1029/2010TC002703>
- Montgomery, D. R., & Foufoula-Georgiou, E. (1993). Channel network source representation using digital elevation models. *Water Resources Research*, 29(12), 3925–3934.
- Rosen, P. A., Gurrola, E. M., Sacco, G., & Zebker, H. A. (2011). InSAR Scientific Computing Environment-The Home Stretch. In *AGU Fall Meeting Abstracts*.
- Tarolli, P., & Dalla Fontana, G. (2009). Hillslope-to-valley transition morphology: New opportunities from high resolution DTMs. *Geomorphology*, 113(1), 47–56. <https://doi.org/https://doi.org/10.1016/j.geomorph.2009.02.006>
- Tofelde, S., Duesing, W., Schildgen, T. F., Wickert, A. D., Wittmann, H., Alonso, R. N., & Strecker, M. (2018). Effects of deep-seated versus shallow hillslope processes on cosmogenic ¹⁰Be concentrations in fluvial sand and gravel. *Earth Surface Processes and Landforms*, 43(15), 3086–3098.

Find out more here:

<https://agupubs.onlinelibrary.wiley.com/doi/full/10.1029/2019JF005141>



Dr. Stephanie Olen

olen@geo.uni-potsdam.de

University of Potsdam,
Institute of Geosciences

Building 27, Room 0.37
Karl-Liebkecht-Str. 24-25
14476 Potsdam-Golm

+49 331 977 2236